CrossMark

ORIGINAL PAPER

Application of particle image velocimetry (PIV) in the study of uplift mechanisms of pipe buried in medium dense sand

Bo Huang[1] · Jingwen Liu[1] · Daosheng Ling[1] · Yanguo Zhou[1]

Abstract Geotechnical centrifuge modeling, which can effectively simulate the stress field of soil in the prototype, was adopted to help investigate the effects of the uplifting of pipes buried at different depths within a medium dense sand under (1) a static state and (2) a dynamic state. To acquire the displacement vector fields and strain contours in the soil around pipes, particle image velocimetry technology was applied. The study focused on the deformation mechanisms of soil surrounding the pipes and ground surface. Two different deformation triggers, external forces and soil liquefaction, were considered. When uplifting was caused by an external force, the relationship between the soil deformation and uplift resistance was similar to the typical ground load–deformation characteristic relationships. There was little displacement of soil during the elastic stage. Along with the uplifting of the pipe, a plastic zone within the range of one pipe diameter (1D) above the pipe appeared in the soil at peak resistance. During the post-peak period, a shear failure plane extended upwards to the ground surface, at an inclined angle forming a trumpet-like shape. The ground surface deformation range expanded according to the buried depth of the pipe. Meanwhile, in a liquefied field, the soil flowed within a heart-shaped region around the pipe. The soil deformation region surrounding a shallow buried pipe, with a width of 5D–6D, was far larger than that found for a pipe buried at the same depth in a static field. Both heave and settlement could be observed on the ground surface.

Keywords Pipeline · Uplift · Soil liquefaction · Deformation mechanisms · Centrifuge test

1 Introduction

Pipelines are the arteries of modern industries and thus contribute to the comfort of urban life. They are widely used in water supply, electricity supply, natural gas transportation lines and communication cables. With the increasing demand for urban land and the requirements of environmental quality, more and more engineering pipelines contributing to the quality of life are buried in the ground. However, pipeline accidents do occur frequently, especially in sandy ground, the results of which may paralyze a city, and even lead to serious secondary disasters [1–3].

According to a large number of surveys [4–7], vertical buckling has been found to be the main failure mode for buried pipelines. The main reasons for this damage are the external forces (caused by thermal and internal pressures, or ground ruptures) and soil liquefaction induced by strong seismic waves. Although both can lead to a rise in the original established positions of the pipes, the mechanisms causing the damage differ, partly owing to differences in the deformation mechanism of the surrounding soil. Engineering design and pipeline support measures are

✉ Daosheng Ling
  dsling@zju.edu.cn

  Bo Huang
  cehuangbo@zju.edu.cn

  Jingwen Liu
  liujingwen198807@163.com

  Yanguo Zhou
  qzking@zju.edu.cn

[1] MOE Key Laboratory of Soft Soils and Geoenvironmental Engineering, Department of Civil Engineering, Zhejiang University, Hangzhou 310058, China

closely related to the soil deformation mechanisms. Hence further study of these deformation mechanisms is of significance in ensuring the safety of pipeline engineering. Necessary are the optimization of design and the targeting of reinforcement measures.

Model tests (under normal gravity or under high gravity) are the principal tools [8, 9] enabling study of the uplifting buckling of pipes. There is a lack, however, of effective model deformation observation methods. In early studies, individual point measurements [10], such as linear variable differential transformer, have been used to capture soil movements at certain positions in the model. With the application of laser displacement sensors, the wider measurement range and the higher test accuracy are guaranteed than before. However, the number of measurement points remains limited. Sometimes, markers such as colored sand layers and plastic rods buried in the soil are used [11], but with a lower measurement precision. The soil deformation mechanism, however, can only be deduced from information obtained at single points or along set up lines by these methods. Based on these earlier studies, several failure mechanisms and a variety of theoretical formulae have been put forward. Trautmann et al. [12] presented a review of formulae for calculating the soil resistance against pipe uplifted. Among them, the most widely used mechanism is the vertical slip-surface model developed by Majer et al. [13]. However, the estimated data according to this mechanism do not match very well with the previous laboratory test [14]. This is because of the insufficient understanding of the soil deformation mechanism.

Hence, it has become clear that there is a need for more advanced measurement methods to investigate the soil deformation mechanism of pipe uplifting as affected by different factors (such as soil properties, pipe buried depth, damage mechanism), to enable the correlation between soil deformation and resistance to be accurately revealed. As the deformation of soil is continuous in space, spatial measurement of soil movement throughout the plane is necessary. Surface measuring methods based on imaging technologies have been gradually developed in recent years. Both the X-ray method [15] and the CT method [16] are included. These techniques can track the internal and external displacements of the prototype model, and can even capture the crack and soil particle shapes. The measuring equipment, however, is very complex and limited in scope, which can hardly be carried out on centrifuge tests. With the promotion of automatic target tracking systems based on image processing techniques [17], this technique was firstly applied in the measurements of soil movement by White et al. [28], named as particle image velocimetry (PIV). It can continuously measure the deformation behavior of a soil surface without artificial targets, also the advantage of high precision and remote control, hence providing a new method for the observation of soil deformations during centrifuge tests.

In the present study, model tests of pipelines uplifted in dry medium dense sand and liquefaction sand were conducted in geotechnical centrifuge, which can simulate the stress field of soil in the prototype. PIV technology was used to observe the soil deformation around a large diameter pipe at different buried depths. The deformation behavior of the ground surface and soil surrounding a pipe during uplifting triggered by different types of disaster was the main concern.

2 Test equipment and programs

2.1 Centrifuge, shaking table and rigid container

Centrifuge modeling techniques are increasingly used to investigate soil–structure interaction. They allow large-scale model tests to be easily carried out in the laboratory. Six tests for this study were conducted using the ZJU400 centrifuge shown in Fig. 1a. The beam type centrifuge, with a payload capacity of 400 gt, has double platforms and an effective arm radius of 4.5 m. The maximum centrifugal acceleration is 140 g for static tests. The centrifuge platforms have an overall dimension of 1.5 m × 1.2 m × 1.5 m. Meanwhile, an 'in-flight' uniaxial electro-hydraulic shaking table is made to simulate seismic excitation, as shown in Fig. 1b. The shaking table has vibration frequencies ranging from 10 to 200 Hz. Its payload capacity is 500 kg, and its maximum lateral displacement and acceleration are 0.6 cm and 40 g, respectively. More details about the device can be found in Ref. [18].

Two rigid containers were used to prepare the models. One container of inner dimension 1 m (length) × 0.45 m (width) × 1 m (height) was for static tests, and the other of inner dimension 0.6 m (length) × 0.4 m (width) × 0.5 m (height) was for dynamic tests. A 25 mm thick piece of moldable Duxseal was placed on each side of the dynamic container to reduce reflecting incident stress waves by at least 65 % [19]. The front perspex made window was convenient for direct observation of the experimental phenomena.
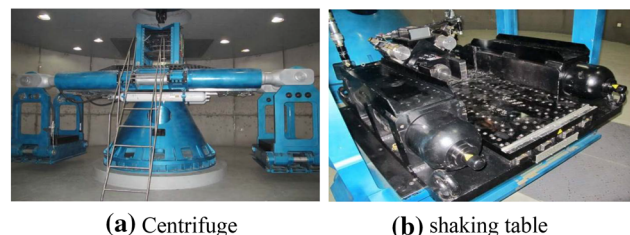

(a) Centrifuge   (b) shaking table

Fig. 1 Centrifuge and shaking table

(a) Force measurement system for Test I

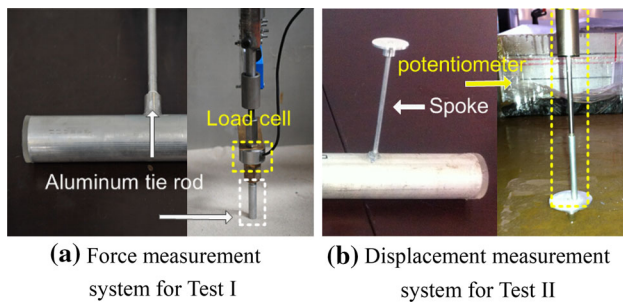**(b)** Displacement measurement system for Test II

Fig. 2 Equipment detail of test I and test II

2.2 Model pipes and transducers

The model pipes used in this study were manufactured from aluminum alloy, with a density of 2.7 g/cm^3 and outer diameter of 40 mm. They simulated large diameter pipes such as those of oil or gas pipelines. The surfaces of the pipes were smooth. At each end, the pipes were sealed by a perspex disc fixed with PTFE to reduce end friction.

In the static tests of pipelines uplifting in dry medium dense sand, displacements of pipe, deformation and resistance of soil were principally measured. The pipe was connected to a vertical actuator through an aluminum tie rod shown in Fig. 2a. A load cell was installed on this rod to measure the uplift resistance of the soil. A laser displacement sensor was used to monitor the vertical displacement of the pipe during tests, as shown in Fig. 3a. The load cell was made by MEAS in the USA with a measuring range and a precision of ±2 kN and 0.3 % full scale output (FSO), respectively. The laser displacement sensor was made by WENGLOR in Germany with a measuring range and a precision of 5 cm and 0.3 % FSO, respectively.

In the dynamic tests of pipelines uplifting in liquefied soil, the ground acceleration response, excess pore water pressure and pipe displacement were the main concerns in this study. A micro pore pressure transducer, which had been saturated and sealed up by petroleum jelly before the tests, was placed at the same depth as the bottom of the pipe to measure the excess pore water pressure. Taken into consideration is that the potentiometer cable, that is commonly used, possesses a tension force which, to some extent, will reduce the structure's self-weight. In fact, the tension force varies with the centrifugal acceleration and is hard to calibrate [20]. Therefore, two aluminum alloy spokes with discs on their ends were installed on the pipe, as shown in Fig. 2b. The vertical displacements of the discs could be measured by potentiometers, which guaranteed a more precise and reliable measurement of the freely moving pipe. The pore pressure transducer was made by DRUCK in Japan with a 700 kPa measuring range and a 0.3 % FSO precision. The potentiometers had a 5 cm measuring range and a 0.3 % FSO precision. The
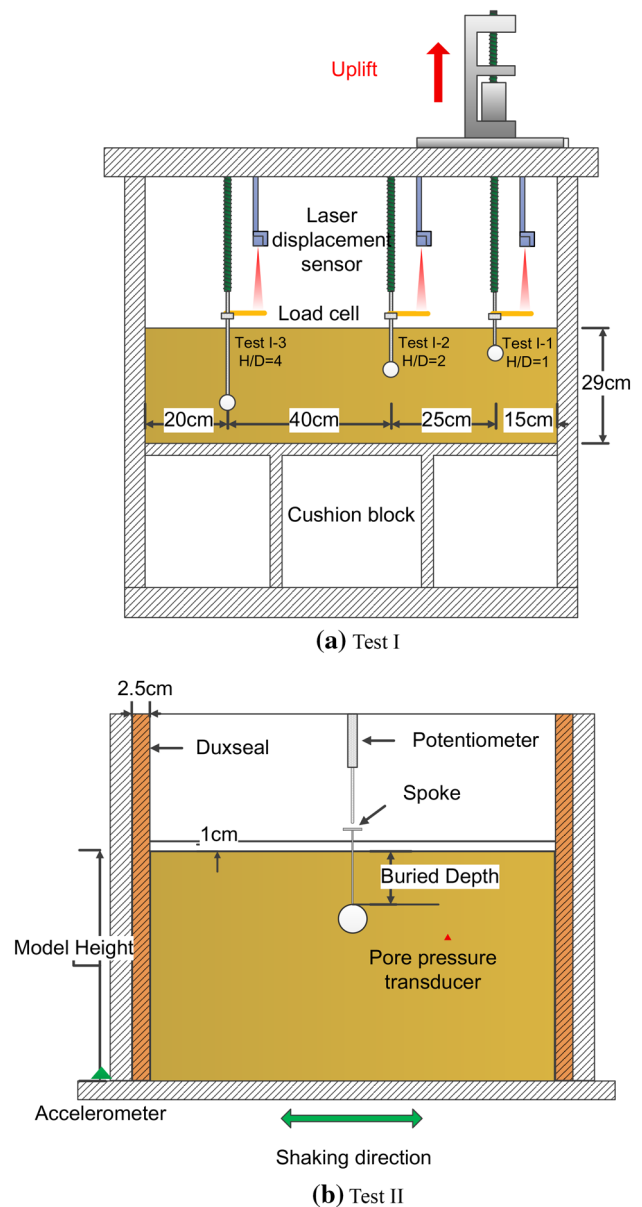

(a) Test I

(b) Test II

Fig. 3 The layout of pipes and sensors

accelerometer was made by KYOWA in Japan with a 100 g measuring range and a 0.2 % FSO precision. To clarify the focus of the study and make the graph more legible, only parts of the transducers used in the tests are shown in Fig. 3b. The layout of the other transducers is given in more detail in Ref. [21].

2.3 Model preparation

Fujian Standard sand, which is widely used in China for geotechnical physical modeling tests [22, 23], was adopted for the present study. It has a mean diameter (D_{50}) of 0.16 mm, an unevenness coefficient (C_u) and a curvature

coefficient (C_c) of 1.6 and 0.95, respectively. The maximum and minimum void ratios are 0.96 and 0.61, respectively. The model foundation was prepared by the pluviation method. The sand was rained from a sieve in a hopper into the container, with the falling height of the hopper and the shape of the sieve kept constant based on pre-calibrated results to obtain a constant relative density. The design relatively density was 60 %.

The static tests were conducted in dry medium dense sand. As the deformation mechanism of dry silica sand was quite similar to the wet one [3, 9], the dry sand condition was chosen to save time. And the buried depths H, from the ground surface to the crown of pipe, were 1D, 2D and 4D (D represents the pipe diameter), respectively. The foundation height of the model was 28 cm. It has already been proved by the previous studies that the width of surface deformation on each side of the pipe mid-line is less than 3D [24, 25]. When the horizontal spacing between two pipes is greater than 6D, there are no interaction effects between them. To ensure that the relative densities of the three models were as consistent as possible, three pipes for the static tests were all buried in the larger rigid box at the same time, as shown in Fig. 3a. The horizontal spacing between the three pipes was 25 and 40 cm, respectively, which met test requirements.

The dynamic tests were conducted in saturated medium dense sand. The buried depths H were 0.5D, 2D and 4D, respectively. The foundation height of the model was 30 cm. There was a conflict between the dynamic and permeability time scales. To solve the problem, methyl cellulose fluid was introduced to reduce the permeability of soil [26]. Methyl cellulose fluid was introduced at a rate of 0.1 L/h into the model foundation when cooling down, which was slow enough to avoid the sand boiling phenomenon. The whole process of saturation took over 200 h and the water level was kept at 1 cm above the ground when the saturation was completed.

2.4 Seismic excitations

To investigate the effect of wave form and amplitude, three types of excitation waves were input, i.e., the EL-Centro wave, the Taft wave and two Zhejiang seismic waves. The El-Centro wave was recorded at the Imperial Valley Earthquake of California in 1940, with a primary period of 0.5 s, relating to a nearby earthquake. The Taft wave was recorded during the Kem Earthquake in California in 1952, with a primary period of 0.5 s, relating to a distant earthquake. These two waves are well-known records [27], commonly used by researchers. The Zhejiang seismic wave is an artificial one, appropriate to the seismic nature of Zhejiang Province in China, with a 10 s duration. The probabilities of these two Zhejiang seismic waves being

exceeded are 10 and 2 %, and their waveforms are a bit different.

2.5 Image analysis

The deformation measurement system based on PIV was used in the tests. PIV is a velocity-measuring technique that was originally developed in the field of experimental fluid mechanics. D. J. White first introduced PIV into geotechnical testing to measure the micro-displacement of soil. The surface of soil model observed is divided into a number of fine patches. The displacement of each patch can be traced by recognizing their textures. The deformation of the whole surface in the spatial scale (which is transformed from the pixel scale by control markers) can be acquired by comparing the coordinates of each patch in the different pictures taken during the tests. More details about the theory are given in Ref. [28].

A Canon G10 camera with the spatial resolution of 4416 pixel × 3312 pixel was used in the tests. This camera could take ten shots a minute, constantly refocusing along the way. A set of black control markers used to calibrate the photogrammetric transformation were fixed between the pipe and the window before the tests. This transformation accounted for camera movement and image distortion. The diameter of the control markers was 3 mm, set about 50 mm apart. To separate the control markers from the soil, white insulating tapes with a diameter of 6 mm were placed behind these markers.

The precision of PIV can be estimated by the following Eq. [28]:

$$\rho_{\text{pixel}} = \frac{6}{L} + \frac{150{,}000}{L^8} \qquad (1)$$

where ρ_{pixel} is a random error and L is length of the patch (which is a square). In the study, the minimum length of the patch was 32 pixels. So the random error was 0.19 pixel, which was 1/17,431 of the spatial resolution of the digital camera. The spatial size of the maximum region taken by the G10 was 500 mm (length) × 420 mm (width). The corresponding random error, therefore, was 0.029 mm. When the acceleration of centrifuge was 30 g, the random error was 0.86 mm in the prototype satisfying the determination accuracy required.

In static tests, the camera was installed on the arm of the centrifuge and was able to meet the test requirements. To make the digital camera and the model box remain relatively static, a camera mounting bracket was used in the dynamic tests. The bracket was fixed on the rigid box, and moved together with it during shaking, shown in Fig. 4a. The distance between lens and box window was 25 cm and which satisfied the measuring requirement. The position of the light source is shown in Fig. 4b.
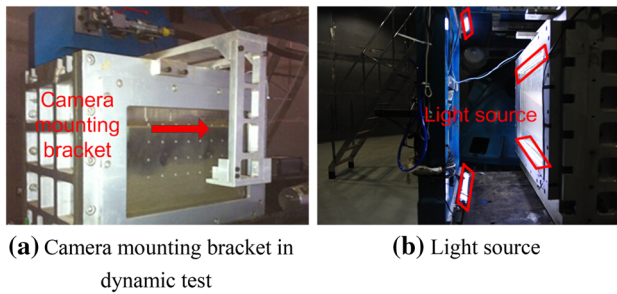
(a) Camera mounting bracket in dynamic test

(b) Light source

Fig. 4 Camera equipment and light source

2.6 Test program

Two categories of centrifuge model tests were conducted, and each category can be subdivided into three conditions based on the buried depth. The detailed information of tests is shown in Table 1.

Category I was static tests of pipelines being uplifted in dry medium dense sand. The uplifting rate of pipes, for the similar studies [14, 29], with a small discrepancy was range from 0.08 to 0.3 mm/min. To simulate the uplifting buckling of a pipe in static state, the pipe was lifted upwards very slowly at a rate of 0.133 ± 0.02 mm/min. When the test started, the centrifuge was accelerated up to 30 g gradually at a rate of 3 g/min. The settlement induced by acceleration was 4 mm, and was uniform throughout the model. After the settlement had remained stable for about 10 min and no abnormal condition occurred, the pipe began to be pulled upwards. After the uplift displacement of the pipe reached 1 cm, the test was finished and the centrifuge was slowed down to a stop.

Category II included dynamic tests of pipelines uplifting in liquefied soil. The centrifuge was first gradually accelerated to 30 g. The settlement induced by acceleration was 5 mm, and was uniform throughout the model. The relative densities of tests II-1, 2, 3 before shaking are shown in Table 1. Although the largest relative density difference among the three tests was 5.3 %, this discrepancy was much less than occurred in previous studies [30, 31] and had little impact on the results. The test results could be

compared. The excitation progress was divided into three stages based on the acceleration amplitudes from weak to strong. White noise excitations were applied before and after each stage to test the fundamental frequency of the model. The schedule of excitations and the uplifting status of test II at each shaking stage are shown in Table 2. There was at least a 30 min interval between any two stages of shaking, so that the excess pore pressure could dissipate entirely. After all excitations had been applied, the test was considered finished along with the centrifuge going down.

The test data given in the sections below are given in model scale, unless specifically stated otherwise. In prototype scale, according to the scaling rules as summarized in Table 3, the length, integrated force, etc. can be increased by the scale-up factor (N or N^2, etc.).

3 Results of tests

3.1 Results of pipe uplifted in dry medium dense sand

3.1.1 Soil deformation mode around pipe

As the sand deformation modes around pipes buried at different depths were quite similar, only the deformation process of test I-2 is given below due to space limitations. Figure 5 shows the displacement vector field calculated by PIV of test I-2 during pipe uplifting (the vectors in the figures are scaled up by a factor of 15 for clarity). With increasing pipe uplift displacement, the soil deformation was firstly observed directly above the pipe crown extending to the ground surface, shown in Fig. 5b. Meanwhile, the deformation region expanded in the horizontal direction gradually, as the region-boundaries changed from curve A to curve B shown in Fig. 5c. A visible trumpet-like deformation could be seen near the ground surface, as curve C shown in Fig. 5d. After the peak resistance, the shear failure zone and the ground heave could be clearly seen. Once the maximum was reached, the deformation region no longer expanded. The sliding region is defined as

Table 1 Summary of tests

Test number	Centrifugal acceleration	H/D	ρ_d (kg/m³)	ρ_{sat} (kg/m³)	I_D (%)	Pipe mass (kg)	H (mm)
I-1	30	1	1502	–	59.2	0.2	40
I-2	30	2	1502	–	59.2	0.2	80
I-3	30	4	1502	–	59.2	0.2	160
II-1	30	0.5	1520	1943	65.2	0.3	20
II-2	30	2	1510	1937	61.9	0.3	80
II-3	30	4	1526	1947	67.2	0.3	160

I_D has considered the settlement induced by the accelerating process of centrifuge

Table 2 Shaking detail and performance of test II [20]

Test no.	Seismic excitation			
	Seismic wave	Duration (s)	Amplitude (g)	Performance of pipe
Test II-1	Noise	1	0.02	
	Zhejiang seism wave (10 %)		0.1	Rise slightly
	EL-Centro		0.1	Remain still
	Noise		0.02	
	Zhejiang seism wave (2 %)		0.15	Sink slightly
	EL-Centro		0.15	Rise slightly
	Noise		0.02	
	EL-Centro		0.5	Rise
	Taft		0.4	Rise
	Noise		0.02	
Test II-2	Noise	1	0.02	
	EL-Centro		0.1	Sink slightly
	Zhejiang seism wave (10 %)		0.1	Remain still
	Noise		0.02	
	EL-Centro		0.4	Rise
	Taft		0.4	Rise
	Noise		0.02	
Test II-3	Noise		0.02	
	EL-Centro		0.1	Remain still
	Zhejiang seism wave (10 %)		0.1	Remain still
	Noise		0.02	
	EL-Centro		0.4	Rise
	Taft		0.4	Rise
	Noise		0.02	

Only the amplitudes of seismic waves are in prototype scale

Table 3 The scaling ratios of the centrifuge modeling

Physical quantity	Dimension	C	Physical quantity	Dimension	C
Length	L	1:N	Velocity	LT^{-1}	1:1
Area	L^2	1:N^2	Acceleration	LT^{-2}	N:1
Volume	L^3	1:N^3	Integrated force	MLT^{-2}	1:N^2
Water content		1:1	Distributed force	ML^{-1}T^{-2}	1:1
Density	ML^{-3}	1:1	Moment of force	ML^{2}T^{-2}	1:N^3
Unit weight	ML^{-2}T^{-2}	N:1	Frequency	T^{-1}	N:1
Cohesive force	ML^{-1}T^{-2}	1:1	Stress	ML^{-1}T^{-2}	1:1
Friction angle		1:1	Strain		1:1
Deforming coefficient	ML^{-1}T^{-2}	1:1	Displacement	L	1:N
Flexural stiffness	ML^{3}T^{-2}	1:N^4	Time	T	
Compressional stiffness	MLT^{-2}	1:N^2	Dynamic process		1:N
Permeability coefficient	LT^{-1}	N:1	Permeability process		1:N^2
Mass	M	1:N^3	Creep process		1:N

N the scale-up factor of acceleration field; C = model/prototype

the instantaneous deformation region shrinks. Figure 6 shows the displacement vector field of test I-2 after a pipe displacement of 0.19D. The vectors in the figures represent the incremental displacements between two images over a time interval of 1200 s. It can be seen that the surrounding sand fell around the pipe periphery to fill the cavity formed beneath the pipe during its uplifting. The sliding region of sand moving along with the pipe became smaller, and its boundaries shrank from curve C to curve D and then to curve E. The sliding region finally became a trapezium

Fig. 5 Displacement vector field of test I-2. *Dash line* represents the original position, *solid line* represents the current position
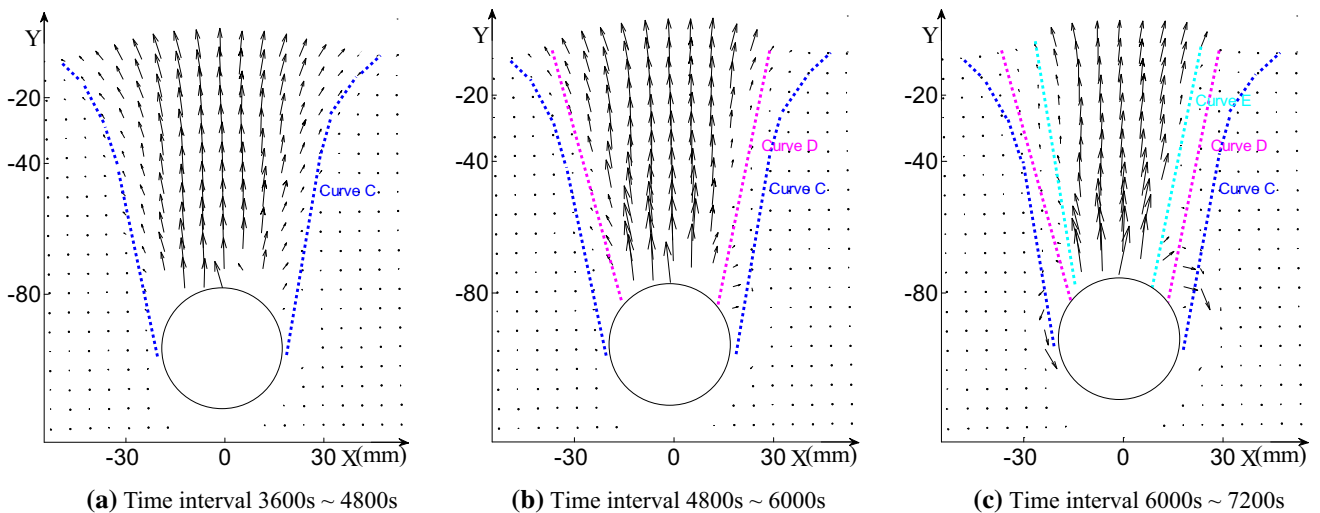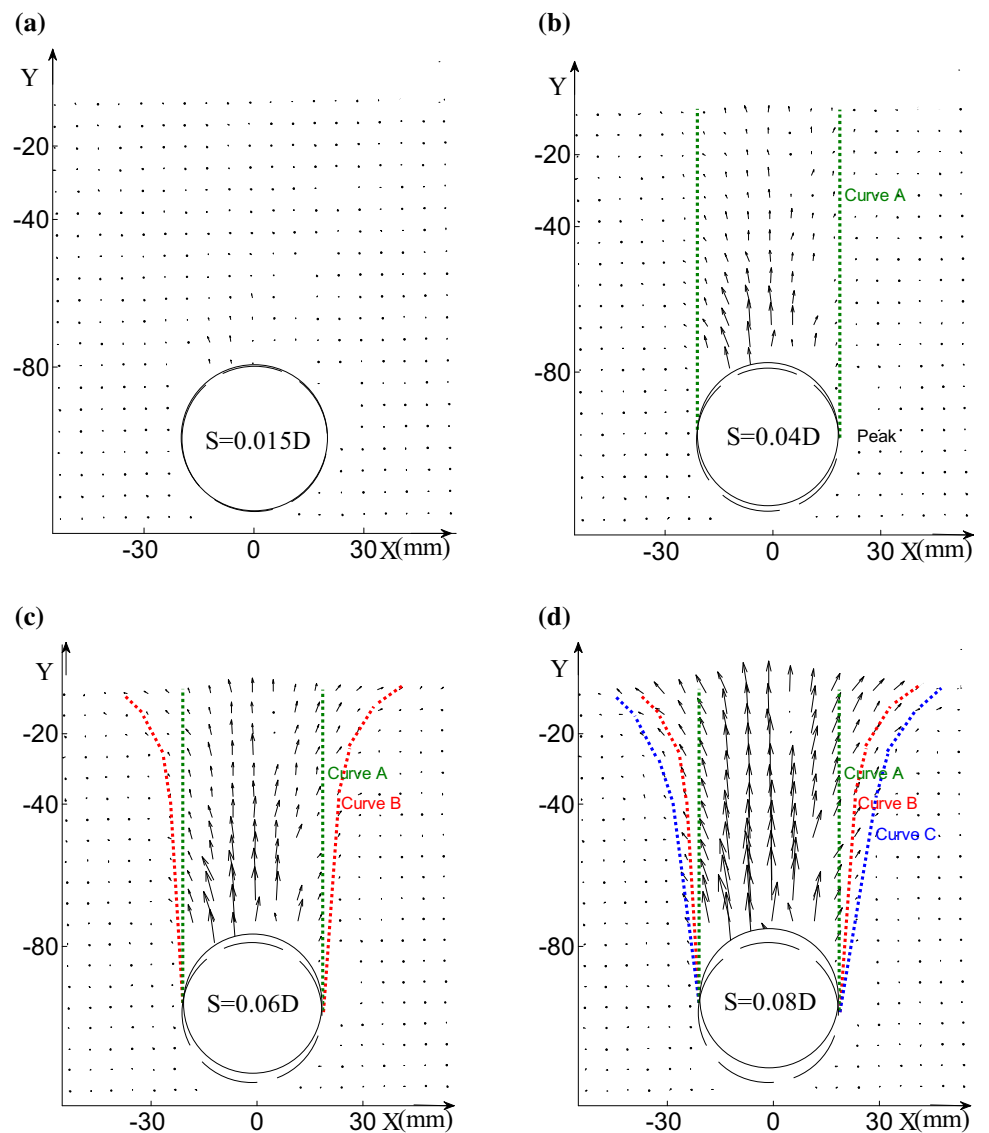

Fig. 6 Sliding region shrinks in unit time during the post-peak period
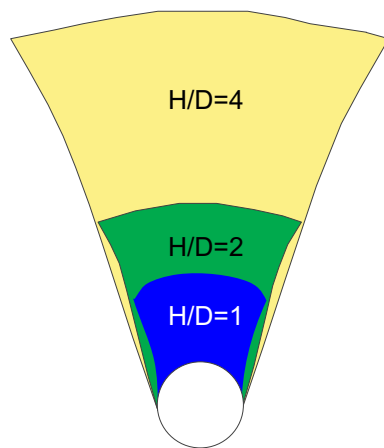
(a) Time interval 3600s ~ 4800s   **(b)** Time interval 4800s ~ 6000s   **(c)** Time interval 6000s ~ 7200s

Fig. 7 Deformation area and slide surface of test I

(a) Test I -1

(b) Test I -3

Fig. 8 *Vertical* displacements above the pipe *centerline*

with 1*D* of topline and 1/2*D* of baseline. As the pipeline upheaval buckling is usually undetectable at the beginning, the shrinking process is difficult to catch in field investigation. Although this phenomenon is not yet explicitly stated, it can be observed in similar model tests [30].

The area enclosed by curve C (the boundary of the maximum deformation region of test I) and the ground surface in the test I series are plotted in Fig. 7. It can be seen that the width of ground heave deformation expanded with increasing depth of burial. The width of the ground heave deformation on each side of the pipe mid-line was 2.4*D* in test I-3, and 2.59 times of test I-1. The widths on each side of the pipe, as stated above, were all less than 3*D*, and were in conformity with previous researches. However, the range of ground upheaval deformation still needs further study for more deeply buried pipeline. Meanwhile, it can be seen that the sliding region shrank more quickly when the buried depth of the pipe is shallower. This was probably because the lateral constraint pressure exerted by soil at a shallow depth was smaller than a greater depth, and the soil layer failing in shear could expand more easily.

The time history curves of vertical displacement ($S_{y.max}$) along the pipe centerline in test I-1 and test I-3 are plotted in Fig. 8. The dashed line represents pipe uplift displacement. It can be seen in test I-1 that the curve of the soil was close to the curve of the pipe for this shallow depth condition. There was only a slight difference (which increased with increasing distance between soil layer and pipe) between the pipe and soil displacement vs. time curves. However, when the pipe was deeply buried, the difference of vertical displacement between soil and pipe was notable. The value of the former was far less than the latter, as shown in Fig. 8b. In the first 500 s of test I-3, the soil above the pipe barely moved while the uplift displacement of the pipe was more than 1 mm. Although the displacement curve of the 0.2*D* soil layer (i.e., 0.2*D* above the pipe
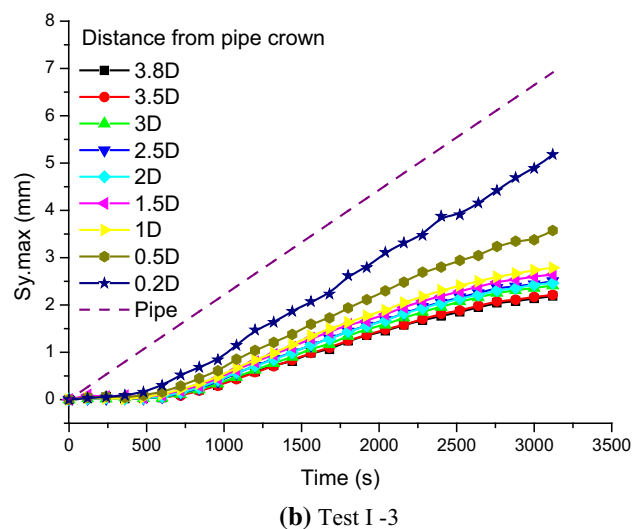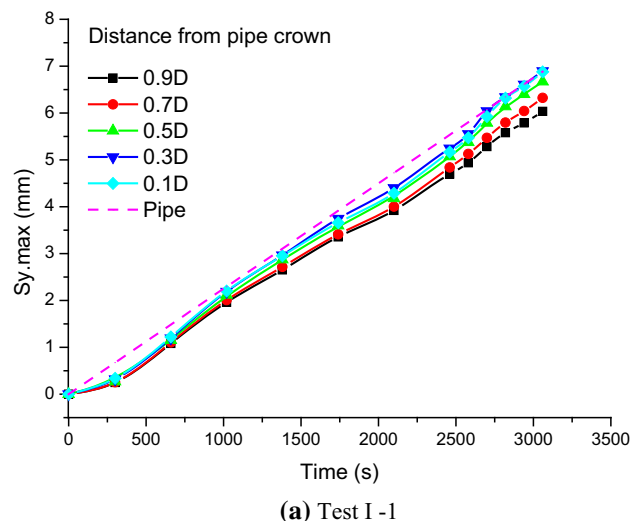
crown) gradually became parallel to the displacement curve of the pipe after 500 s, the difference in movements between pipe and soil remained obvious for the soil at some distance from the pipe. This means compression in the soil was noteworthy above a deeply buried pipe.

The displacement vector field revealed the range and the shape of the ground deformation region, but it could not reflect changes in soil strain. To investigate the soil deformation mechanism in more detail, the strain variation of soil is discussed in the next section.

3.1.2 Strain and strain rate of soil around pipe

Through PIV analysis, the actual coordinates of each patch in the pictures taken during tests can be acquired. The compression strain in the soil in the *y* direction and the shear strain can be obtained using these coordinates. The calculation method is detailed in "Appendix".

The contours of shear strain γ_{xy} and compression strain in the y direction ε_y for test I-3 are plotted in Figs. 9 and 10, respectively. It can be seen that most of the surrounding soil was in an elastic state in the early stage of pipe uplifting, and the shear deformation and compression deformation were concentrated only around the surface of pipe. The strain contours in test I-3 at a pipe moving displacement of 0.015D are shown in Figs. 9a and 10a.
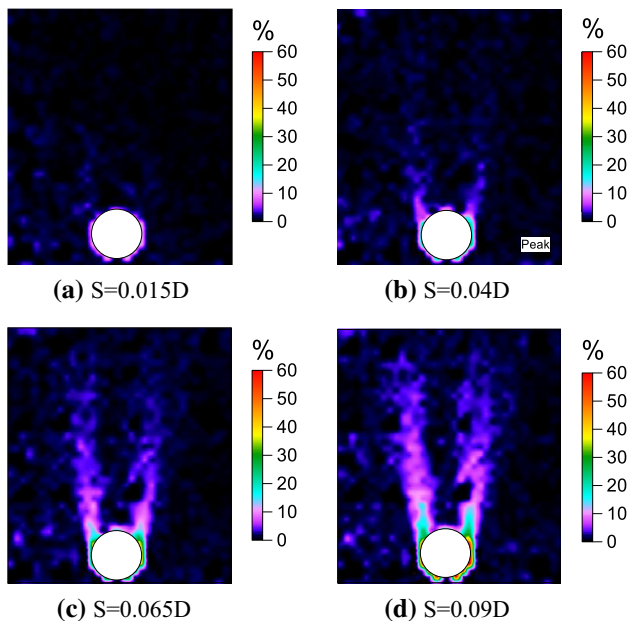

Fig. 9 Shear strain of soil during uplift in test I-3
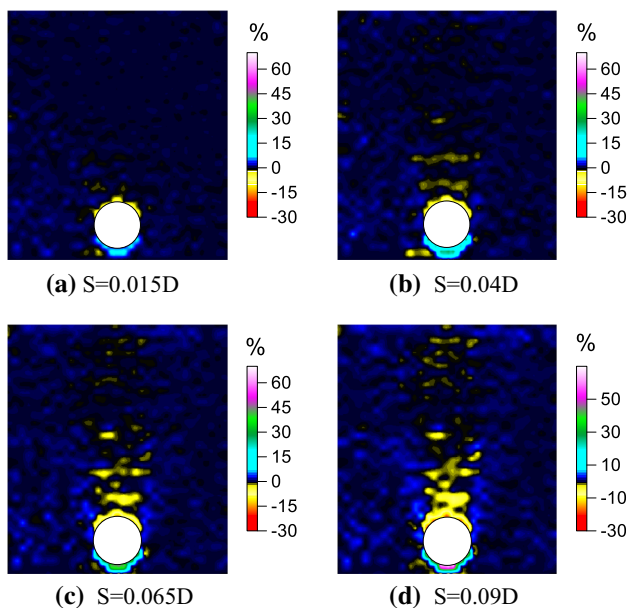
Fig. 10 Compression strain of soil during uplift in test I-3

The shear strain γ_{xy} and compression strain ε_y could be observed in the soil above the pipe along with the pipe uplift value. The shear strain zone was inclined and extended upwards to the ground surface, indicating the plastic zone formed, as shown in Fig. 9d. The compression strain ε_y mostly appeared in the inverted trapezoid-like soil block between the shear zones and also developed upwards to the ground surface, as shown in Fig. 10b–d. Although the displacement vector fields for the three tests in category I at peak resistance were different, their strain contours were quiet similar. The plastic zones were all distributed within a 1D range above the pipe, as shown in Figs. 9b and 10b. When the soil resistance reached its peak value, the maximum shear strain generally ranged from 5 to 8 %.

The shear bands in the soil propagated at an accelerating rate after the peak, and finally extended upwards to the ground surface. Based on analyses of the displacement vector fields and strain contours, the sliding region, looked like an inverted trapezoid, moved upwards with pipe. This was in accordance with the sliding block mechanism theory used in the calculation of soil resistance [28]. It is worth mentioning that the sliding block was not rigid. In addition to its shrink in size, compression existed within the sliding block.

The $\gamma_{xy\cdot max}$ (the maximum shear strain at each depth) of the soil above the pipe at different depths in test I-2 are plotted in Fig. 11. In the first 300 s, the $\gamma_{xy\cdot max}$ value was only distributed from 0 to 0.5 %. There was little difference between the maximum shear strains at each depth, and the corresponding soil resistance curve followed in a linear pattern at the same time, as shown in Fig. 12. The soil was still in a state of elastic deformation. After 300 s, the $\gamma_{xy\cdot max}$ became quite different. The shear strain of the soil developed faster for the soil closer to the pipe. Part of the soil above the pipe was in a plastic state. There seemed to be a link between the rates of decline of soil uplift resistance and shear strain during the post-peak period. As the maximum shear strain remained stable, the soil resistance dropped very slowly during the period 2000s–2900s in Figs. 11 and 12. Because of the periodical squeezing, shearing and crushing of soil particles, the shear strain rate fluctuated during pipe uplifting. The magnitude of the shear strain rate was small, basically ranging from ±0.01 %/s, as shown in Fig. 13.

The value of $\varepsilon_{y\cdot max}$ (the maximum compression strain at a certain depth) and the compression strain rate in the soil above the pipe for different depths in test I-3 is plotted in Fig. 14. It can be seen that the compression strain was mostly concentrated in the soil up to a 10 cm above the pipe. The compression strain rate also fluctuated during pipe uplifting and ranges within ±0.005 %. These phenomena were also observed in the other two tests.
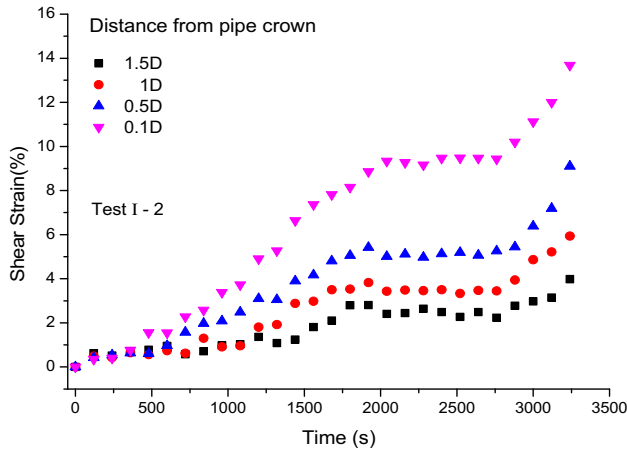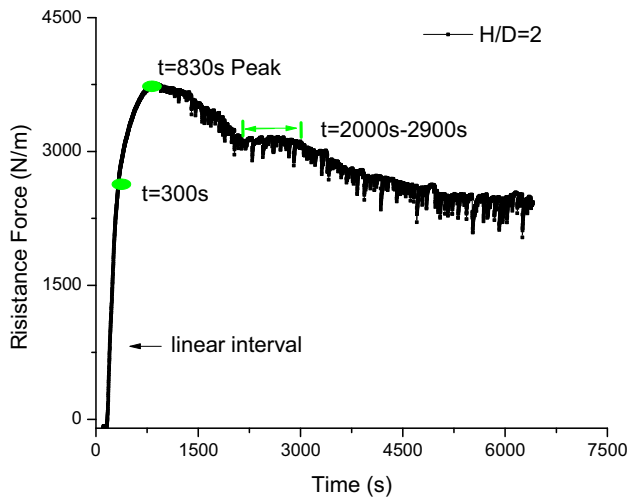
Fig. 11 Shear strain of test I-2

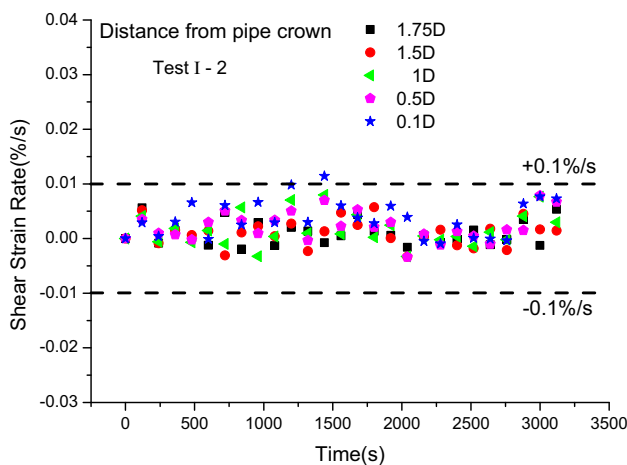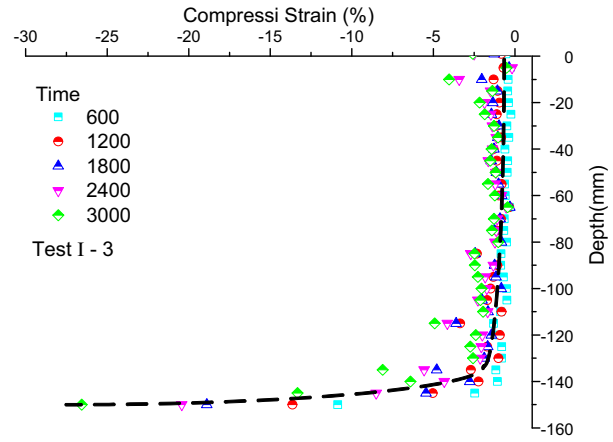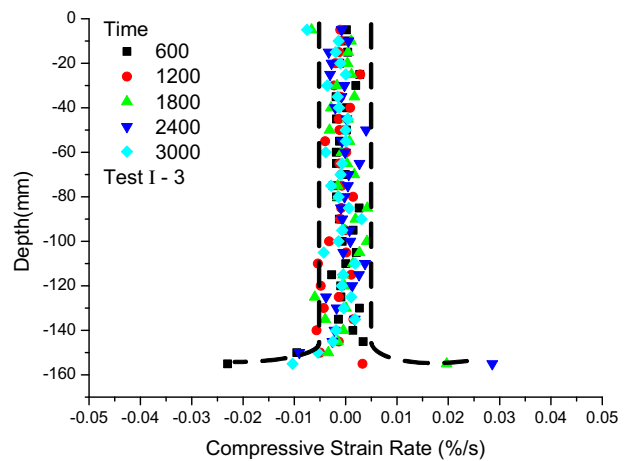
Fig. 12 Force–displacement *curve*

Fig. 13 Shear strain rate of test I-2

(a) The maximum compression strain of soil above pipe

(b) The maximum compression strain rate of soil above pipe

Fig. 14 Compression strain and compression strain rate of test I-3

3.2 Results of pipe uplift in liquefied sand

3.2.1 Uplifting displacement of pipe

The failure mechanism of pipe induced by soil liquefaction is different from the vertical uplifting of a pipe caused by external forces (such as thermal and internal pressure actions, or ground ruptures). The loss of shear strength of the soil due to build-up of excess pore pressure results in pipeline instability. Sinking or floatation failure mode can both take place during liquefaction.

The vertical displacement vs. time curves of pipes in the series of category II tests under 0.4 g (or 0.5 g) El-Centro wave are shown in Fig. 15. Herein, negative values of displacement mean that the pipe settles down, and positive values represent uplift. As the vertical displacement tendencies of pipes subjected to other waves with different amplitudes were similar, the other test results are not given below owing to space limitation. It can be seen that the
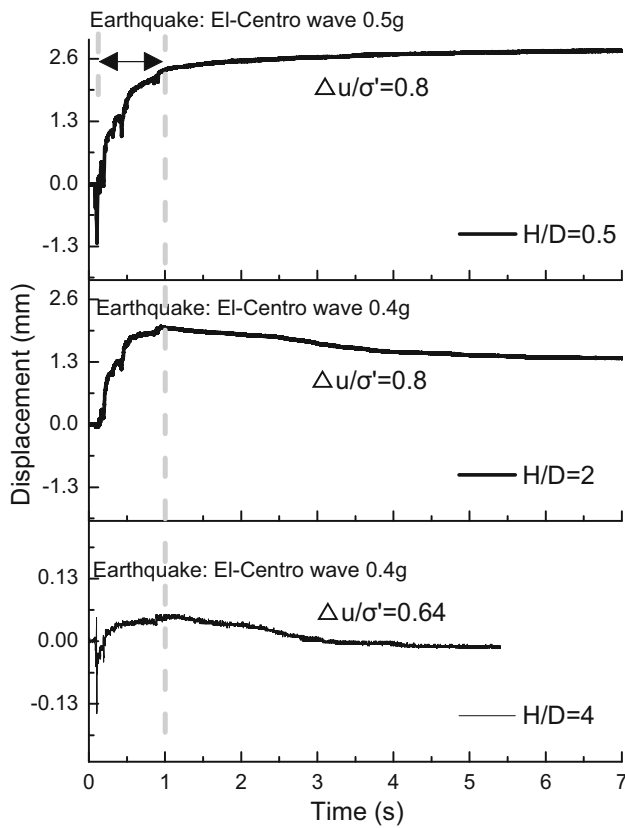
Fig. 15 Uplift displacement of pipeline of test II during El-Centro wave shaking

pipe settled immediately at the beginning of shaking. The pipe soon recovered to its original position due to the elasticity of the sand. The pipe then started to rise. When the shaking ceased, the vertical displacement of the pipe went on increasing slightly or decreasing.

Some researchers hold the view that the uplifting of the pipe is highly dependent on the input earthquake motion, and weakly relates to the increase of excess pore water pressure [32, 33]. It seems according to the tests that this view may be confirmed as the uplifting phenomenon of pipe occurred during the shaking. Through the records measured by the pore pressure transducer, the uplifting movement was determined not only by the shaking itself but also in response to the extra pore water pressure. The uplifting displacement of pipe was closely related to the build-up of pore pressure in the ground.

The excess pore pressure ratio $\Delta u / \sigma'_{v0}$ defined as the value of the excess pore pressure Δu (measured by pore pressure transducer at the same depth as the bottom of pipe) normalized by the initial vertical effective stress σ'_{v0} represents the degree of soil liquefaction. The vertical displacement vs. time curve and the excess pore pressure ratios vs. time curve in test II-2 under the El-Centro wave with different amplitudes are plotted in Fig. 16. It can be
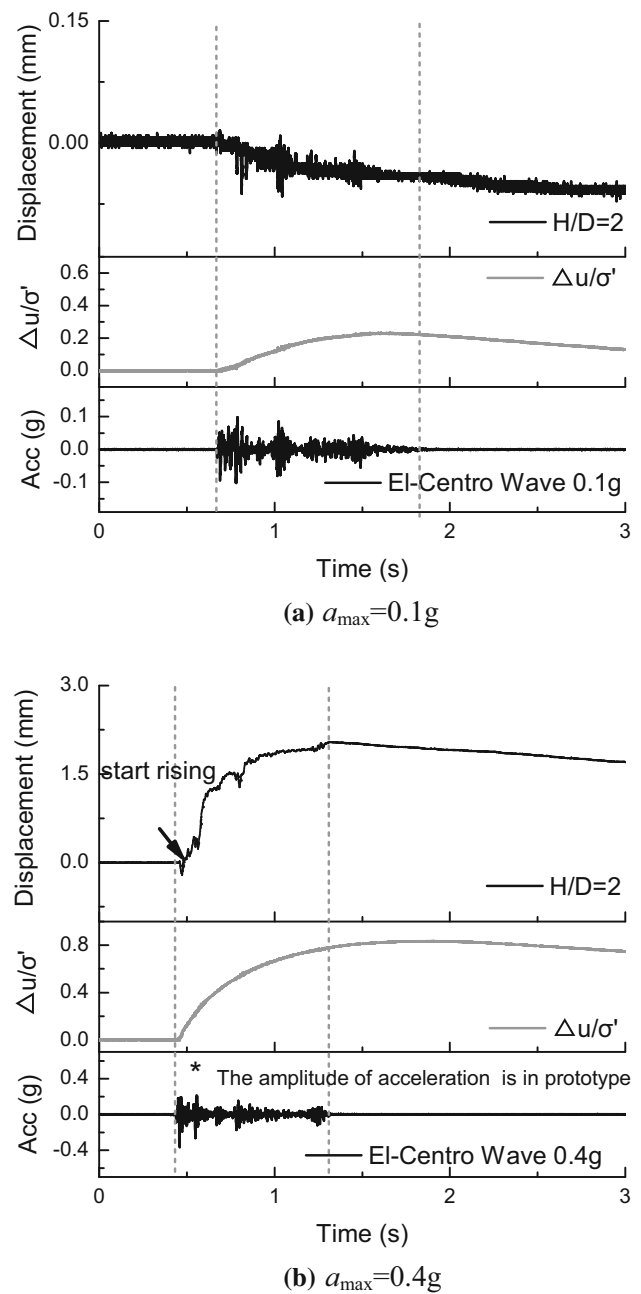

Fig. 16 Uplift displacement of pipeline of test II-2 during El-Centro wave shaking

seen that the uplifting of the pipe did not take place immediately after the vibration start. Moreover, when the maximum excess pore pressure Δu_{max} was small, the pipe was settled along with the soil particles rather than uplifting as shown in Fig. 16a. The relationship between the maximum uplifting displacement of the pipe and the maximum excess pore pressure ratio $\Delta u / \sigma'_{v0max}$ obtained during tests under each shaking is shown in Fig. 17. Apparently, uplifting of the pipe occurred when the maximum excess pore pressure ratio $\Delta u / \sigma'_{v0max}$ exceeded a
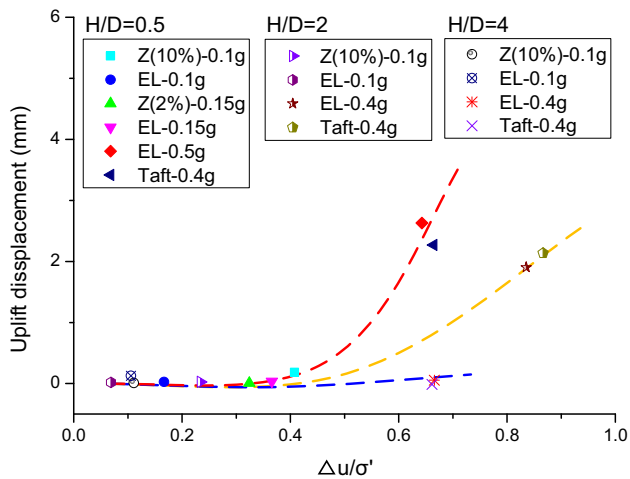
Fig. 17 Relationship among uplift displacement, $\triangle u / \sigma'$ and excitation

threshold which relates to the pipe buried depth. Uplifting of the pipe took place when $\Delta u / \sigma'_{v0\max}$ exceeded 0.4 for 0.5D buried depth condition. An insignificant displacement appeared when $\Delta u / \sigma'_{v0\max}$ exceeded 0.64 for 4D buried depth condition. The uplifting displacement of the pipe buried to a certain depth was related by a power function relationship to excess pore pressure. It can be seen that the uplifting displacement was larger when the buried depth of the pipe was shallower for the same excess pore pressure ratio.

3.2.2 Soil deformation image analysis

As the frequency of camera shots was limited, the soil deformation process during dynamic tests could not be captured. However, by PIV analysis comparing the two pictures taken before and after shaking, the soil deformation behavior due to that shaking could be acquired. The soil deformation mechanism of the soil around the pipe in a liquefied field is analyzed below.

The deformation modes of the soil surrounding a pipe induced by liquefaction and axial force were quite different. Figure 18a, b presents the displacement vector field of test I-1 and test II-2 at a pipe displacement of 0.18D. It can be seen in Fig. 18a that the width of influence on the soil when pipe was uplifted in test I-1 was just 1.5D. The wedge-shaped sliding block was moving upwards along with the pipe and the soil outside the block was barely influenced. The width of influence on the soil was smaller when the buried depth of the pipe was shallower. Meanwhile, the soil flowed in a circle around the pipe when the pipe uplifted in liquefied ground, as shown in Fig. 18b. The width of ground upheave deformation was about 2.5D. At a distance of 1.25D from the pipe center, the ground settled

followed by upheaving. The width of soil influenced by the circular flow underground surface could reach even as far as to 5D, far more than the influence width on the soil in Fig. 18a. Apart from deformation observed above the pipe, the soil beneath the pipe, for a distance of about 1D, also deformed.

As the soil deformation flow path was incomplete because the buried depth of pipe in test II-1 was too shallow, the displacement vector field of the soil in test II-2 under the EL-Centro wave ($a_{\max} = 0.4$ g) is plotted as supplementary in Fig. 19 (the vectors in the figure is scaled up by a factor of 5 for clarity). The soil directly above the pipe was raised by the uplifting pipe. At the distance above the pipe crown of about 1D, the soil gradually moved away from the pipe's centerline and replaced the soil which had moved into the displaced void beneath the pipe. The soil beneath the pipe was disturbed for a distance of about 1D. The flow tendency around the pipe was more obvious in soil near to the pipe than far away from it. The soil around the pipeline flowed in a heart-shaped region from top to bottom of the field. At a distance of about 3D from each side of the pipe centerline, all the soil was involved in the circular flow. Within the heart-shaped region, a small elliptically shaped closed loop was located at each side of the pipe shoulder at a distance 0.25D. The soil within the closed loop had almost no displacement while the soil between the pipe and the closed loop moved upwards along with the pipe and soil away from the pipe flowed down around the surface of the closed loop. In a liquefied field, apart from the soil deformation within the range of influence of the circular flow, settlement of soil still existed outside this range. As for test II-1, the settlement was largest at the ground surface. A similar circular flow deformation mechanism was observed by Yasuda and Kiku [34] during field investigations in 2004 Niigataken-Chuetsu Earthquake in Japan.

These typical characteristics described above were different from the deformation of soil around a pipe uplifting in static ground, as the mechanisms causing damages were different. When vertical uplifting of pipe was caused by an external force, the soil above pipe was lifted as a wedge-shaped block and shear failure mainly occurred between soil particles. The influence range of the failure was small. When the ground was liquefied during shaking, however, the soil properties had greatly changed. With an increasing degree of soil liquefaction, the soil was transformed into a fluid gradually. When uplifting failure of the pipe took place, the soil above the pipe could not move upward as a block. The pipe uplifting was highly dependent on such as the build-up of the excess pore pressure, the shear strength of the soil, the seismic wave characteristics, etc. This type of damage occurred in a short time, and quite a large area around the pipe could be affected.

Fig. 18 Deformation mode of soil surrounding pipe under different trigging reason
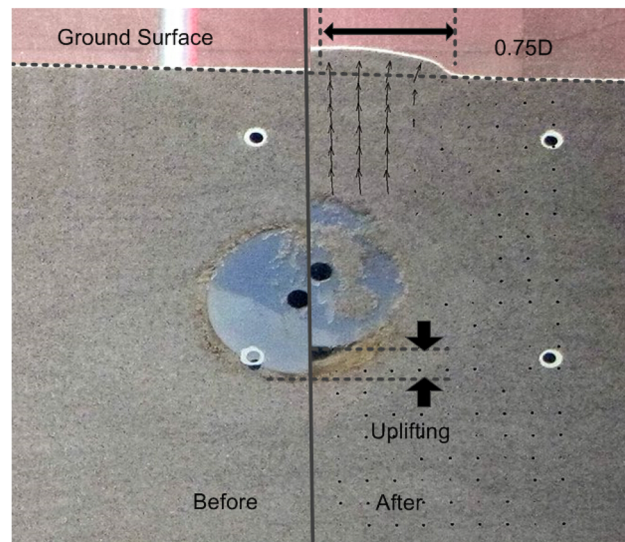
(a) Test I -1
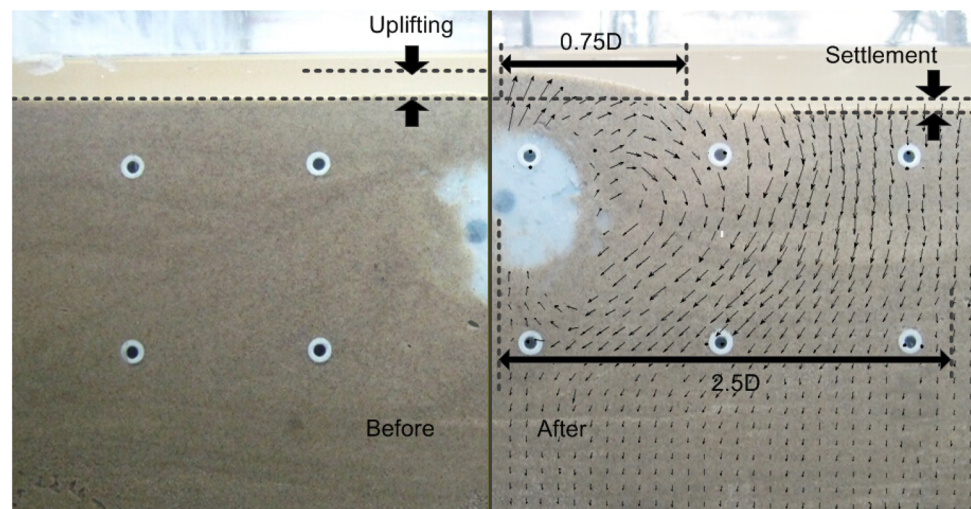
(b) Test II -1

The buried depth for test II-3 was greater than for the other two category II tests. That the uplifting displacement was very small and the circular soil flow deformation did not appear is evident from Fig. 20 (the vectors in the figure are scaled up by a factor of 10 for clarity). This was caused by the heavy weight of the soil above the pipe and the low degree of liquefaction. As the amount of data were limited, critical excess pore pressure ratio causing pipe uplift for different buried depths could not be deduced. However, it was certain that the greater the pipe buried depth the better the ground stability during liquefaction induced by an earthquake. Obvious vibration deformation in the ground is also seen in Fig. 20, to be quite different to that of tests II-1 and II-2. The ground soils in the latter two cases, as stated above, were more affected by the buried pipe and the deformation mode was symmetrical along the pipe centerline. However, in test II-3, the deformation was more inclined to resemble the response of a free-field to an earthquake and was less influenced by the presence of the pipe.

4 Conclusions

Through centrifuge model tests, the deformation behaviors of medium dense soil around a buried pipe induced by (1) external forces (such as thermal and internal pressure actions, or ground ruptures) and (2) by soil liquefaction were studied. The deformation mechanisms and the areas around the pipeline affected by those deformations under these two types of damages were quite different.

When the pipe uplifts due to external forces, at first strains were only observed in the soil above the pipe for a
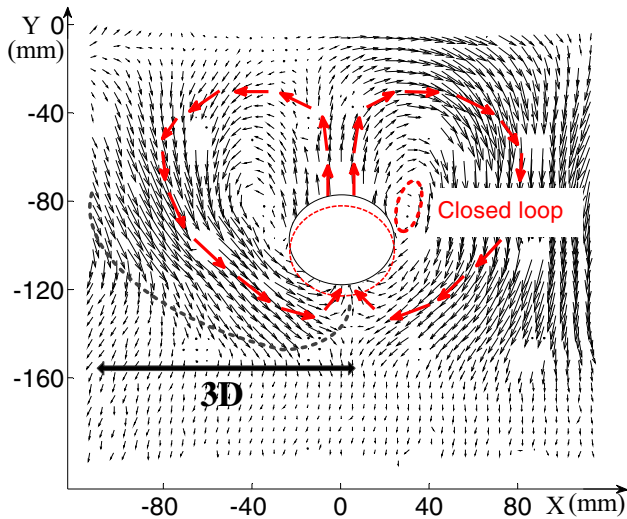
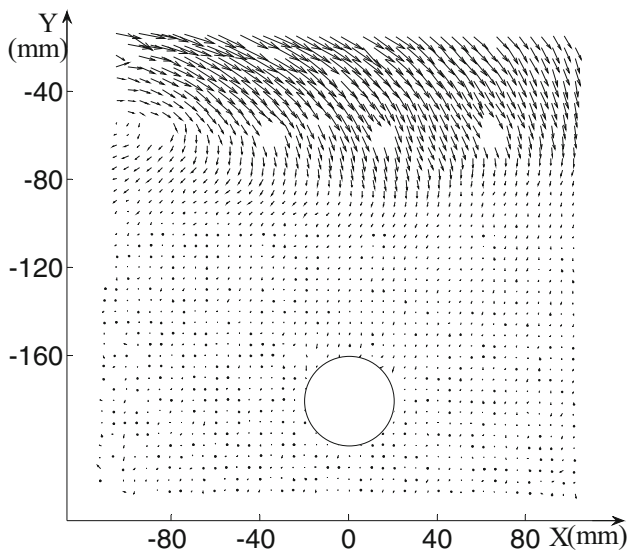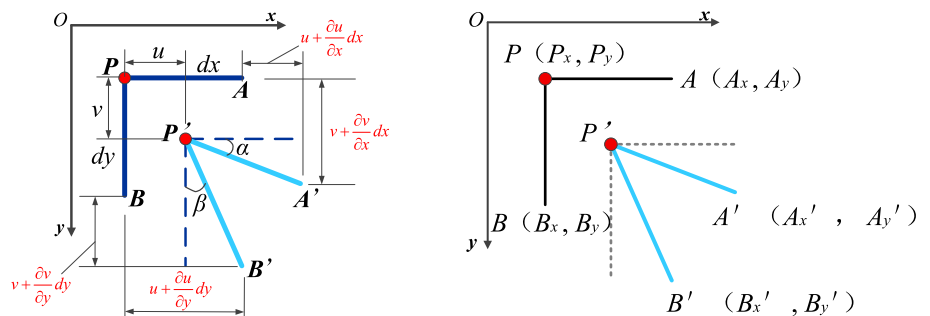**Fig. 19** Soil displacement vector field in test II-2 under EL-Centro wave ($a_{max} = 0.4$ g)

Fig. 20 Soil displacement vector field in test II-3 under EL-Centro wave ($a_{max} = 0.4$ g)

failure plane with an inclined angle extended upward to the ground surface. A trumpet shaped deformation reached the ground surface. In the resistance—softening stage, the soil beside the pipe shoulder fell around the pipe periphery reducing the size of the sliding soil block. The range of the ground surface deformation expanded with increasing pipe buried depth. In the study reported here, the widths of ground surface deformation on each side of the pipeline were all less than 3D.

In the case of a liquefied soil due to earthquake, the soil around the pipeline gradually flowed around the pipe within a heart-shaped region. The deformation range of the soil at the surface in the case of shallow buried pipe was about 5D–6D, greater than that due to external forces for the same buried depth. The soil beneath the pipe could also be disturbed during uplifting. Both upheaval and settlement deformation could be observed at the ground surface, but the uplifting behavior of a pipe was highly dependent on the build-up of excess pore pressure. Only when the value $\Delta u / \sigma'_{v0_{max}}$ exceeded a threshold which relate to the pipe buried depth, could the pipe started to float. The uplifting displacement of a pipe was related to excess pore pressure ratio by a power function.

Appendix

The actual coordinates of each patch on the observation surface can be obtained through a PIV analysis. Each patch is regarded as a mass point. Every four adjoining mass points can constitute a rectangular soil element. As the deformation of the soil element is symmetrical [35], only three points in the rectangular soil element are needed to calculate the shear strain and normal strain.

Figure 21 illustrates that point P, point A and point B move to the position of P', A' and B' respectively. The

distance of about 1D. The shear strains generally ranged between 5 and 8 % at peak soil resistance. Along with the uplifting of the pipe during the post-peak period, a shear

Fig. 21 Relationship between geometric strain deformation and coordinates

displacements of the three points are indicated in the figure. Point P is taken at location (P_x, P_y), and the displacement components of this point are thus u and v. The corresponding displacements of point A are $u + \frac{\partial u}{\partial x}dx$ and $v + \frac{\partial v}{\partial x}dx$ while the displacements of point B are $u + \frac{\partial u}{\partial y}dy$ and $v + \frac{\partial v}{\partial y}dy$ based on the small deformation theory. The normal strain in the x direction can thus be defined by

$$\varepsilon_x = \frac{u + \frac{\partial u}{\partial x}dx - u}{dx} = \frac{\partial u}{\partial x}. \qquad (2)$$

In similar fashion, the normal strain in the y direction becomes

$$\varepsilon_y = \frac{v + \frac{\partial v}{\partial y}dy - v}{dy} = \frac{\partial v}{\partial y}. \qquad (3)$$

For small deformations $\tan \alpha \approx \alpha$ and $\tan \beta \approx \beta$, and the shear strain can then be expressed as:

$$\gamma_{xy} = \alpha + \beta = \frac{v + \frac{\partial v}{\partial x}dx - v}{dx} + \frac{u + \frac{\partial u}{\partial y}dy - u}{dy} = \frac{\partial v}{\partial x} + \frac{\partial u}{\partial y}. \qquad (4)$$

Combined the coordinates of the points and the formulae of strain derived before, the coordinate expression of strain can be expressed as:

$$\varepsilon_x = \frac{(A'_x - P'_x) - (A_x - P_x)}{(A_x - P_x)} \qquad (5)$$

$$\varepsilon_y = \frac{(B'_y - P'_y) - (B_y - P_y)}{(B_y - P_y)} \qquad (6)$$

$$\gamma_{xy} = \frac{(A'_y - P'_y) - (A_y - P_y)}{(A_x - P_x)} + \frac{(B'_x - P'_x) - (B_x - P_x)}{(B_y - P_y)}. \qquad (7)$$

In the present study, the contours of ε_y and γ_{xy} of soil are described in detail. And the negative value of ε_y in the paper represents the compression strain of soil.

References

1. O'Rourke TD, Gowdy TE, Stewart HE, Pease JW (1991) Lifeline and geotechnical aspects of the 1989 Loma Prieta earthquake. In: Proceedings of 2nd international conference on recent advances in geotechnical earthquake engineering and soil dynamics. University of Missouri-Rolla, Rolla, pp 1601–1612. http://hdl.handle.net/10355/42283. Accessed 8 Aug 2013
2. Majid Z, Mohsin R (2012) Failure investigation of natural gas pipeline. Arab J Sci Eng 37(4):1083–1088. doi:10.1007/s13369-012-0236-z
3. Bransby MF, Ireland J (2009) Rate effects during pipeline upheaval buckling in sand. Geotech Eng 162(5):247–256. doi:10.1680/geng.2009.162.5.247
4. Taylor N, Tran V (1996) Experimental and theoretical studies in subsea pipeline buckling. Mar Struct 9(2):211–257. doi:10.1016/0951-8339(94)00021-J
5. Hobbs R (1984) In-Service buckling of heated pipelines. J Transp Eng 110(2):175–189. doi:10.1061/(ASCE)0733-947X(1984)110:2(175)
6. Maltby TC, Calladine CR (1995) An investigation into upheaval buckling of buried pipelines-II. Theory and analysis of experimental observations. Int J Mech Sci 37(9):965–983. doi:10.1016/0020-7403(95)00005-I
7. Saeedzadeh R, Hataf N (2011) Uplift response of buried pipelines in saturated sand deposit under earthquake loading. Soil Dyn Earthq Eng 31(10):1378–1384. doi:10.1016/j.soildyn.2011.05.013
8. Sumer BM, Fredsøe J, Christensen S, Lind MT (1999) Sinking/floatation of pipelines and other objects in liquefied soil under waves. Coast Eng 38(2):53–90. doi:10.1016/S0378-3839(99)00024-1
9. Bransby M, Newson T, Brunning P, Davies M (2001) Numerical and centrifuge modelling of the upheaval resistance of buried pipelines. In: Proceedings of 20th international conference on OMAE, Rio de Janeiro
10. Ng CW, Li X-S, Van Laak PA, Hou DY (2004) Centrifuge modeling of loose fill embankment subjected to uni-axial and bi-axial earthquakes. Soil Dyn Earthq Eng 24(4):305–318. doi:10.1016/j.soildyn.2003.12.002
11. Liu R, Yan S, Wu X (2012) Model test studies on soil restraint to pipeline buried in Bohai soft clay. J Pipeline Syst Eng Pract 4(1):49–56. doi:10.1061/(ASCE)PS.1949-1204.0000109
12. Trautmann CH, O'Rourfce TD, Kulhawy FH (1985) Uplift force–displacement response of buried pipe. J Geotech Geoenvironmental 111(9):1061–1076. doi:10.1061/(ASCE)0733-9410(1985)111:9(1061)
13. Bransby M, Newson T, Brunning P (2002) Centrifuge modelling of the upheaval capacity of pipelines in liquefied clay. In: Proceedings of ISOPE, Kitakyushu, pp 100–107. https://www.isope.org/publications/proceedings/ISOPE/ISOPE%202002/Volume2/2015p100.pdf. Accessed 3 Mar 2014
14. White D, Barefoot A, Bolton M (2001) Centrifuge modelling of upheaval buckling in sand. Int J Phys Model Geotech 1(2):19–28. doi:10.1680/ijpmg.2001.1.2.19
15. Butterfield R, Harkness R, Andrews K (1970) A stero-photogrammetric method for measuring displacement fields. Géotechnique 20(3):308–314. doi:10.1680/geot.1970.20.3.308
16. Heijs AW, De Lange J, Schoute JT, Bouma J (1995) Computed tomography as a tool for non-destructive analysis of flow patterns in macroporous clay soils. Geoderma 64(3):183–196. doi:10.1016/0016-7061(94)00020-B
17. Paikowsky S, Fan X (2000) Particle motion tracking utilizing a high-resolution digital CCD camera. ASTM Geotech Test J 23(1):123–134. doi:10.1520/GTJ11130J
18. Chen MY, Han C, Ling DS, Kong LG, Zhou YG (2011) Development of geotechnical centrifuge ZJU400 and performance assessment of its shaking table system. Chin J Geotech Eng 33(2):1887–1894 (In Chinese)
19. Steedman R, Madabhushi S (1991) Wave propagation in sand medium. In: Proceedings of 4th international conference on seismic zonation. Stanford University, Palo Alto
20. Chian SC (2012) Floatation of underground structures in liquefiable soil. Dissertation, University of Cambridge
21. Huang B, Liu JW, Lin P, ling DS (2014) Uplifting behavior of shallow buried pipe in liquefiable soil by dynamic centrifuge test. Sci World J. doi:10.1155/2014/838545
22. Han C, Zhou YG, Chen YM (2010) Numerical simulation of centrifuge-shaking table test on saturated sand. Proc Int Conf E-Prod E-Serv. doi:10.1109/ICEEE.2010.5660350

23. Fan JY (2013) Pile–soil–pile interaction in pile groups subjected to eccentric lateral loading. Dissertation, Zhejiang University (in Chinese)

24. Abduljauwad SN, Al-Ghamedy HN, Siddiqui JA, Asi IM, Al-Shayea NA (2004) Stability of vertically bent pipelines buried in sand. J Press Vess-T 126(3):382–390. doi:10.1115/1.1767858

25. Ghaly A, Hanna A, Hanna M (1991) Uplift behavior of screw anchors in sand. I: dry sand. J Geotech Eng 117(5):773–793. doi:10.1061/(ASCE)0733-9410(1991)117:5(773)

26. Yang D, Naesgaard E, Byrne PM, Adalier K, Abdoun T (2004) Numerical model verification and calibration of George Massey Tunnel using centrifuge models. Can Geotech J 41(5):921–942. doi:10.1139/t04-039

27. KiKusawa M, Hasegawa T (1985) Analysis of model embankment dam by shaking table test. Soils Found 25(1):1–14. doi:10.3208/sandf1972.25.1

28. White DJ, Take WA, Bolton MD (2003) Soil deformation measurement using particle image velocimetry (PIV) and photogrammetry. Géotechnique 53(7):619–631. doi:10.1680/geot.2003.53.7.619

29. Wang J, Haigh SK, Forrest G, Thusyanthan NI (2012) Mobilization distance for upheaval buckling of shallowly buried pipelines. J Pipeline Syst Eng Pract 3:106–114. doi:10.1061/(ASCE)PS.1949-1204.0000099

30. Cheuk CY, White DJ, Bolton MD (2005) Deformation mechanisms during uplift of buried pipes in sand. In: Proceedings of 16th international conference on soil mechanics and geotechnical engineering, Osaka, vol 2, pp 1685–1688. http://www-civ.eng.cam.ac.uk/geotech_new/people/bolton/mdb_pub/163_ICSMGE_OSAKA_2005_Vol2_1685-1688.pdf. Accessed 3 Jun 2014

31. Ling HI, Mohri Y, Kawabata T, Liu H, Burke C, Sun L (2003) Centrifugal modeling of seismic behavior of large-diameter pipe in liquefiable soil. J Geotech Geoenvironmental 129(12):1092–1101. doi:10.1061/(ASCE)1090-0241(2003)129:12(1092)

32. Chian SC, Tokimatsu K (2012) Floatation of underground structures during the M_w 9.0 Tōhoku earthquake of 11th March 2011. In: Proceedings of 15th WCEE, Lisboa. http://www.iitk.ac.in/nicee/wcee/article/WCEE2012_3705.pdf. Accessed 26 Aug 2014

33. Sun L (2001) Centrifuge modeling and finite element analysis of pipeline buried in liquefiable soil. Dissertation, Columbia University

34. Yasuda S, Kiku H (2006) Uplift of sewage manholes and pipes during the 2004 Niigataken-Chuetsu earthquake. Soils Found 46(6):885–894. doi:10.3208/sandf.46.885

35. Sadd MH (2005) Elasticity: theory, application, and numeric. Elsevier Butterworth-Heinemann, Burlington